ELSEVIER

Earth and Planetary Science Letters 148 (1997) 193–205

EPSL

Trace element transport during dehydration processes in the subducted oceanic crust: 1. Experiments and implications for the origin of ocean island basalts

Tetsu Kogiso [a,b,*], Yoshiyuki Tatsumi [c], Satoshi Nakano [d]

[a] *Department of Earth and Planetary Sciences, Tokyo Institute of Technology, Ookayama 2-12-1, Meguro, Tokyo 152, Japan*
[b] *Department of Geology and Mineralogy, Faculty of Science, Kyoto University, Kyoto 606-01, Japan*
[c] *School of Earth Sciences, Faculty ofIntergrated Human Sciences, Kyoto University, Yoshida-Nihon-Matsu, Kyoto 606-01, Japan*
[d] *National Institute for Research in Inorganic Materials, 1-1 Namiki, Tsukuba, Ibaraki 305, Japan*

Received 16 November 1995; revised 30 December 1996; accepted 15 January 1997

Abstract

Dehydration experiments on natural amphibolite have been carried out under upper mantle P/T conditions, in order to examine transportation of trace elements during dehydration processes in the subducted oceanic lithosphere. Pb, Nd, and Rb are more readily transported by aqueous fluids during amphibolite dehydration than U–Th, Sm, and Sr, respectively. The results indicates that the dehydration of subducted oceanic crust may result in large increases in U/Pb, Th/Pb and Sm/Nd ratios, and a decrease in Rb/Sr ratios of subducted oceanic crust. This ultimately leads to higher Pb and Nd isotopic ratios, and lower Sr isotopic ratios in the subducted oceanic crust than the present MORB source mantle, given a sufficiently long periods of isolation in the mantle. It follows that the very high Pb isotopic ratios observed in some ocean island basalts, known as HIMU, can be readily achieved by incorporation of ancient subducted crust into their mantle source. However, Sr and Nd isotopic ratios cannot be explained by bulk mixture of the ancient subducted oceanic crust with depleted or primitive mantle, but require significant fractionation of Nd/Sr ratios in the subducted oceanic crust before mixing with mantle material. Possible processes to produce Sr and Nd isotopic compositions similar to that of HIMU may involve partial melting of recycled subducted basaltic crust under lower mantle conditions and refertilization of primitive mantle by the partial melt.

Keywords: ocean-island basalts; trace elements; dehydration; subduction; chemical fractionation

1. Introduction

Dehydration of the subducted oceanic crust in subduction zones is one of the important processes of element fractionation operating in the Earth. Aqueous fluids released by dehydration play an essential role in subduction zone magmatism and crustal formation [1], and dehydrated oceanic crust sinking into the deep mantle may produce chemical heterogeneity in the mantle, especially in the source region of ocean island basalts (OIBs) [2]. It has been speculated that the subducted oceanic crust may contribute to the formation of OIB sources in the deep mantle, based on Sr, Nd and Pb isotopic ratios and trace

* Corresponding author. Fax. +81 3 5499 2094. E-mail: kogiso@geo.titech.ac.jp

PII S0012-821X(97)00018-6

element signatures [3–5] and Re–Os isotope systematics [6,7]. However, an essential problem with the origin of OIB mantle sources is the production of high U/Pb and Th/Pb ratios that are required to develop the extremely high Pb isotopic ratios observed in so-called HIMU OIBs [8], because relative mobility of U, Th and Pb during dehydration processes under subduction zone P/T conditions has not been evaluated.

Brenan et al. [9,10] have documented mineral–aqueous fluid partition coefficients for minerals present in the subducted oceanic crust for U, Pb and some incompatible elements, and suggested that U/Pb and Th/Pb ratios in subducted oceanic crust may increase after dehydration in subduction zones. However, element transport during actual dehydration processes in subducted oceanic crust would be more complicated than simple mineral–fluid equilibrium partitioning. Dehydration reactions in actual subduction zones would occur under rather "open" conditions, because the H_2O fluid phase released by dehydration migrates upwards into the overlying mantle. Moreover, incompatible elements in the mantle and subducted lithosphere may be distributed not only in mineral phases but also along grain boundaries [11,12], which are possible "phases" to retain elements incompatible both to fluid and residual solid phases [13,14].

In this study we have carried out dehydration experiments on a "natural" amphibolite under "open system" conditions, which are analogous to processes operating in subducted oceanic crust. We have investigated trace element transport during amphibolite dehydration, and made a critical assessment based on these data as to whether the dehydrated oceanic crust is a plausible source material to account for the parent/daughter ratios and isotopic composition of HIMU.

2. Experimental and analytical procedures

2.1. Starting material

The oceanic crust, with a bulk composition equivalent to MORB, is commonly metamorphosed to greenschist facies by hydrothermal activity at mid-oceanic ridges and subsequent interaction with sea water during residence on the ocean floor [15]. The principal hydrous phases developed in the metamorphosed oceanic crust are amphibole, epidote and chlorite [1,16]. Upon subduction into the upper mantle, the metamorphosed oceanic crust transforms from a greenschist assemblage via amphibolite to eclogite; through chlorite and epidote decomposition to hornblende, which, in turn, decomposes to garnet and clinopyroxene [16,17]. Hornblende is the most abundant hydrous phase in the subducted oceanic crust [18,19], and thus the transformation of amphibolite to eclogite may be primarily responsible for releasing aqueous fluids from the subducted oceanic crust. We therefore sought hornblende-dominant amphibolite starting material for dehydration experiments.

Natural amphibolite from Iratsu in the Sanbagawa metamorphic belt (Shikoku, Japan) was selected as a starting material for this study. The modal and chemical compositions of the starting material are listed in Tables 1 and 2, respectively. The amphibolite consists of predominantly hornblende, albite, and epidote, with minor amounts of muscovite, garnet, rutile, apatite, quartz, and Fe-oxide minerals, along with small amounts of Fe–Cu-sulfide minerals. This mineral assemblage represents metamorphic conditions of amphibolite facies, which are expected in subducted oceanic crust [17]. Muscovite may also be stable in K-rich basaltic rocks under amphibolite facies [15]. The starting material is enriched in K_2O (0.74 wt%) relative to average N-MORB (~0.1 wt%), consistent with the observation that oceanic

Table 1
Modal compositions of starting materials and run products

Mineral (vol%)	Amphibolite	Mineral (vol%)	Run products (average)
Hornblende	68.1	Omphacite	48.2
Albite	15.0	Garnet	29.1
Epidote	8.9	Phengite	14.3
Muscovite	4.9	Coesite	8.1
Garnet	2.6	Rutile	0.3
Rutile	0.3		
Apatite	0.1		
Fe-oxides	0.1		
Quartz	tr		
Sulfides	tr		

Determined by point counting for amphibolite (5000 points), and element mapping for run products (1000 × 1000 pixels). *tr* = trace.

Table 2
Chemical compositions of starting materials

	Amphibolite	s.d.	Range of altered MORB
SiO_2 (wt%)	48.53		41.63–52.30
TiO_2	0.38		0.41–2.25
Al_2O_3	13.76		13.20–17.95
Fe_2O_3	7.49		1.40–5.09
FeO	8.72		3.92–11.03
MnO	0.21		0.04–0.37
MgO	7.48		5.80–13.23
CaO	7.66		2.78–13.30
Na_2O	2.52		0.57–4.48
K_2O	0.74		0.02–8.16
P_2O_5	0.21		0.03–0.27
$H_2O(-)$	0.05		
$H_2O(+)$	2.34		
Total	100.09		
Li (ppm)	42.7	0.5	3–75
Be	0.94	0.00	
Sc	43.6	0.4	26–171
Ti	12365	75	
V	377	19	170–290
Cr	95.0	4.7	195–800
Co	41.6	1.5	26–60
Ni	53.9	1.4	70–250
Cu	64.6	0.8	12–295
Zn	121	3	
Rb	17.2	0.3	0.32–66.8
Sr	179	4	30–310
Y	47.2	0.6	22–59
Nb	10.2	0.2	2.5–12
Cs	0.91	0.00	0.004–1.15
Ba	61.5	2.1	1–150
La	8.9	0.2	0.9–11
Ce	22.3	0.1	2.5–28
Pr	3.4	0.1	0.72–2.17
Nd	16.7	0.2	4.3–14
Sm	5.3	0.1	1.4–4.4
Eu	1.8	0.0	0.52–1.7
Gd	6.8	0.0	2.2–5.55
Tb	1.2	0.0	0.43–1.1
Dy	7.8	0.2	2.72–6.25
Ho	1.7	0.0	0.61–1.35
Er	4.8	0.0	1.72–3.86
Yb	4.4	0.1	1.70–3.71
Lu	0.7	0.0	0.3–0.8
Ta	0.7	0.0	0.05–1.1
Pb	6.8	0.0	< 2–55
Th	0.7	0.0	0.038–0.122
U	0.4	0.0	0.01–0.669
S	< 5		

Major elements were measured by a wet chemical technique. Chemical compositions of altered MORB are taken from [44–48]. *s.d.* = 1 standard deviation.

crust could be enriched in K by hydrothermal alteration at mid-oceanic ridges [20]. Moreover, the amphibolite shows no evidence of secondary alteration, such as secondary veins and clay minerals. It is thus suggested that the mineral assemblage of the starting material is similar to that of subducted oceanic crust. The major element composition of the starting material is within the range of altered MORB, indicating that residual mineral assemblage remaining upon dehydration of the amphibolite may also be similar to that of actual dehydrated oceanic crust. The concentrations of trace elements in the amphibolite are also in the range of altered MORB (Table 2).

2.2. High-pressure experiments

Finely powdered (< 200 mesh) starting materials were wrapped in perforated platinum foil to enable escape of any H_2O fluid liberated during the course of the experiments. The experiments were carried out in a belt-type high-pressure apparatus with a 32 mm diameter pressure chamber. The pressure medium and graphite furnace include pyrophyllite, NaCl + 10 wt% ZrO_2, and BN sleeves and plugs. The configuration is illustrated in Fig. 1. The oxygen fugacity was not buffered. Pressure was calibrated at room temperature by means of the known pressure-induced phase transitions of Bi (2.55 GPa), Tl (3.67 GPa), and Ba (5.5 GPa). Temperature was estimated from the extrapolated relations between the input

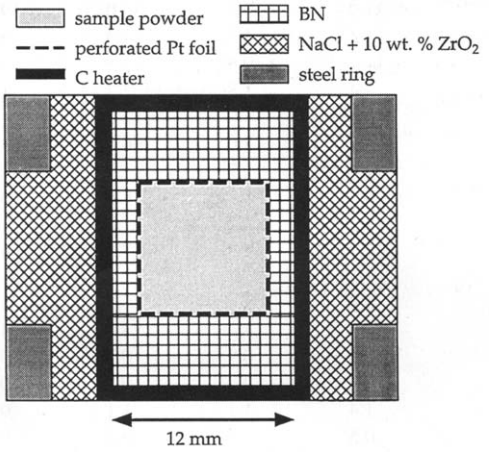

Fig. 1. Configuration of high pressure assembly for the present experiments.

power and the temperature, the latter being obtained in advance by measuring temperatures up to 1020°C with chromel–alumel thermocouples. No correction was made for the pressure effect on the electromotive force of the thermocouples. Temperature uncertainty was within ±15°C. All experiments were conducted at 5.5 GPa and 900°C for 20 h, well above the stability limit of hornblende. The temperature was increased to run temperature at a rate of 45°C/min and, as a consequence, the dehydration reactions of hornblende and the other hydrous minerals present will have occurred almost simultaneously, in contrast to the actual subduction process wherein chlorite and epidote will dehydrate prior to hornblende [16]. After quenching, the pressure was reduced and the sample was recovered.

2.3. Trace element analyses

We analyzed the dehydrated cores of run products, following washing in distilled H_2O for 15 min in an ultrasonic bath. The margins (~ 1 mm) were removed prior to analysis to avoid the effect of the tiny amounts of melt present in some experiments,

Table 3
Chemical compositions of run products and calculated mobilities of trace elements

Element	Amphibolite						Standard		
(ppm)	N145	N189	N166	N182	N195	N194	BCR-1 PV	BCR-1 M	s.d. (%)
Li	41.2	39.3	38.7	38.7	39.4	38.1	12.9	13.9	1.0
Be	0.88	0.86	0.86	0.72	0.86	0.88	1.60	1.79	0.90
Sc	45.1	45.5	43.7	45.2	44.0	43.7	32.6	33.1	1.7
Ti	11937	11981	11946	12525	12097	11066	13429	13458	5
V	358	405	350	363	395	383	405	411	7
Cr	96.1	95.3	93.0	96.1	93.0	91.6	16.0	8.9	1.5
Co	44.6	40.8	41.4	44.3	44.7	44.2	37.0	37.9	1.0
Ni	54.2	54.7	52.7	54.7	53.9	52.4	13.0	11.5	1.4
Cu	40.4	33.7	32.5	28.0	31.4	31.0	19.0	15.4	1.3
Zn	123	127	122	121	120	126	129	134	2
Rb	9.7	4.9	8.2	4.6	6.6	5.2	46.9	48.0	1.0
Sr	116	110	121	82	114	108	327	323	1
Y	48.3	48.5	48.1	49.4	48.9	48.3	37.0	39.0	1.3
Nb	9.9	9.9	10.1	10.3	10.2	9.8	12.5	13.0	1.0
Cs	0.46	0.50	0.51	0.22	0.57	0.50	0.96	0.98	1.42
Ba	31.9	29.0	36.0	19.2	32.5	30.8	675.0	682.6	0.8
La	5.4	3.3	4.5	3.5	4.0	3.3	24.9	25.2	1.0
Ce	14.4	9.6	12.5	10.4	11.3	9.4	53.6	53.0	0.8
Pr	2.4	1.8	2.2	1.9	2.0	1.7	6.8	6.8	1.0
Nd	12.7	11.0	12.5	11.8	12.1	10.8	28.8	28.7	0.9
Sm	4.7	4.6	4.8	4.8	4.7	4.7	6.6	6.6	1.1
Eu	1.7	1.7	1.7	1.7	1.7	1.7	2.0	1.9	0.4
Gd	6.5	6.7	6.6	6.8	6.7	6.7	1.1	6.6	0.9
Tb	1.2	1.2	1.2	1.2	1.2	1.2	6.7	1.1	0.7
Dy	7.7	7.7	7.5	8.0	7.7	7.8	6.4	6.3	1.7
Ho	1.7	1.7	1.6	1.7	1.6	1.7	1.4	1.3	1.2
Er	4.9	4.9	4.7	5.0	4.8	4.8	3.7	3.7	0.7
Yb	4.5	4.4	4.3	4.6	4.4	4.4	3.4	3.3	0.6
Lu	0.7	0.7	0.7	0.7	0.7	0.7	0.5	0.5	0.4
Ta	0.7	0.7	0.7	0.7	0.7	0.7	0.8	0.8	1.5
Pb	1.4	1.1	1.1	0.8	1.0	0.9	13.5	13.0	0.4
Th	0.5	0.5	0.5	0.4	0.5	0.5	5.9	6.2	0.4
U	0.3	0.3	0.3	0.2	0.3	0.3	1.6	1.7	0.9
S							< 5		

Table 3 (continued)

Mobility (%)	N145	N189	N166	N182	N195	N194	Average	s.d.
Li	5.8	10.3	11.6	11.6	10.0	12.8	10.4	2.5
Be	8.3	10.6	10.9	25.3	11.1	9.0	12.5	6.4
Sc	−1.0	−1.9	2.0	−1.2	1.5	2.1	0.3	1.8
Ti	5.7	5.4	5.6	1.1	4.5	12.6	5.8	3.8
V	7.1	−5.0	9.2	5.8	−2.4	0.8	2.6	5.7
Cr	1.2	2.1	4.4	1.2	4.4	5.9	3.2	2.0
Co	−4.6	4.3	2.9	−3.9	−5.0	−3.7	−1.7	4.1
Ni	1.7	0.9	4.5	0.8	2.2	4.9	2.5	1.8
Cu	38.9	49.1	50.9	57.7	52.5	53.1	50.4	6.3
Zn	0.7	−2.1	1.4	2.7	3.8	−1.2	0.9	2.3
Rb	44.8	72.4	53.7	74.2	62.5	70.3	63.0	11.7
Sr	36.7	39.9	34.0	55.0	37.9	41.2	40.8	7.4
Y	0.1	−0.4	0.6	−2.2	−1.0	0.1	−0.5	1.0
Nb	4.9	4.5	3.3	1.4	2.0	5.7	3.6	1.7
Cs	50.6	46.5	45.8	76.6	38.6	46.6	50.8	13.2
Ba	49.3	54.0	42.7	69.5	48.4	51.1	52.5	9.1
La	40.9	63.5	51.3	61.2	56.3	63.6	56.1	8.8
Ce	36.9	57.9	45.3	54.4	50.8	59.1	50.7	8.4
Pr	32.3	48.2	36.9	44.4	41.9	50.6	42.4	6.9
Nd	25.7	35.6	26.8	31.0	29.4	36.9	30.9	4.6
Sm	13.9	15.3	12.9	12.0	13.4	14.1	13.6	1.1
Eu	9.5	7.5	8.0	5.0	9.6	9.8	8.3	1.9
Gd	7.1	4.1	6.5	3.2	4.5	4.7	5.0	1.5
Tb	3.5	0.2	3.2	0.0	1.3	0.3	1.4	1.6
Dy	4.0	4.0	5.9	0.8	4.1	2.7	3.6	1.7
Ho	2.8	2.3	4.5	0.2	3.9	3.2	2.8	1.5
Er	0.3	−0.3	3.6	−2.7	2.0	0.7	0.6	2.1
Yb	0.4	2.4	3.6	−2.7	2.0	2.7	1.4	2.3
Lu	0.3	−0.1	2.4	−3.8	0.8	−1.8	−0.4	2.1
Ta	0.5	−1.3	0.0	−1.8	−1.2	1.5	−0.4	1.3
Pb	79.2	84.1	84.1	88.0	85.0	87.0	84.6	3.1
Th	28.2	37.4	35.6	50.5	36.5	38.0	37.7	7.2
U	25.2	27.5	25.1	41.3	27.9	27.9	29.1	6.1

BCR-1 PV = preferred values; BCR-1 M = measured values for standard BCR-1. *s.d.* = 1 standard deviation.

possible contamination with the capsule material, and the possible concentration of mobilized materials due to incomplete liberation of H_2O fluid from the capsule.

The run product of each experiment was analyzed along with multiple analyses of the starting material. The trace element compositions of both the starting material and run products were determined along with an international standard (BCR-1) by ICP–MS, following the method of Eggins et al. [21]. Detection limits are typically 1 ppb or better for most elements reported, except Li, Sr, and Pb, which are in the range 10–100 ppb, and Ti, V, Cr, Co, Ni, Cu, and Zn which are generally in the range 0.1–1 ppm. Sulfur compositions of the amphibolite and a dehydrated run product were analyzed by iodometric titration at Muséum National d'Histoire Naturelle, France, following the method of Lorand [22].

3. Results and discussions

3.1. Run products

The dehydration experiments were performed six times under the same temperature–pressure condition and duration. The run products were analyzed using an optical microscope, X-ray powder diffraction and an electron microprobe analyzer. Modal composition of the run products were determined by

element mapping (1000 × 1000 pixels), using the electron microprobe analyzer (Table 1). Hornblende was completely decomposed in all run products, and the mineral assemblage remaining after dehydration comprised omphacite, garnet, phengite, coesite, and rutile. This mineralogy is consistent with that expected for the subducted basaltic crust at 5.5 GPa, where garnet and clinopyroxene dominate [23], and with phengite stable below at least 6 GPa and 900°C [19,24]. The run products contain 12 vol% phengite (Table 1), equivalent to about 0.4 wt% H_2O. This means that 80% of H_2O present in the starting material was lost through the perforations in the capsule.

Tiny amounts of glass were found at the margins of some experimental charges (N166 and N189). The thickness of melted parts is less than 200 μm, where no phengite was found. In contrast, the cores of these charges showed no evidence of melting, and contain significant amounts of phengite. Phengite in basaltic systems disappears rapidly just above the solidus, with increasing temperature at higher pressures [24]. It is thus suggested that temperatures of the cores of the charges were lower than the solidus, whereas the margins were above the solidus because of possible temperature gradients in the charges. It is unlikely that partial melts in the charges were removed through the perforation of the Pt capsule because the glasses at the margins have high SiO_2 contents (> 85 wt%). It follows that no glass in the cores indicates that the cores of the charges did not undergo partial melting. We analyzed only the cores of the run products after removing the melted margins, so we conclude that the element mobilities described below are not affected by partial melting at the margins.

3.2. Mobilities of trace elements

The analytical results of the starting material and the run products are listed in Tables 2 and 3. All run products display a similar compositional contrast to the starting materials, although the absolute concentrations are somewhat variable due to variations in the efficiency of element transport out of these open-system experiments (Table 3). The Ni concentration is equivalent in the starting materials and run products, indicating that significant element loss from residual solid phases to the Pt capsule by solid-state diffusion did not occur in the charges. It follows that element loss from the residual phases was controlled by element dissolution to fluid phases; that is, element mobilities may reflect their abilities to dissolve in fluid phases (see below).

The mobility of an element during the dehydration experiments can be expressed as the percentage of an element removed by aqueous fluids during dehydration reactions as follows:

$$\text{Mobility} = \frac{C_{STM} - C_{RP}}{C_{STM}} \times 100(\%)$$

where C_{STM} and C_{RP} are the concentrations of an element in the starting material and in the run products, respectively.

The mobilities of incompatible trace elements are plotted in Fig. 2. Large-ion lithophile elements (LILEs: Cs, Rb, Ba, Pb, Sr, U and Th) and light rare earth elements (LREEs) were more effectively transported by the aqueous fluid. It should be noted that the mobility of Pb is exceptionally high relative to other LILEs. In contrast, high-field strength elements (HFSEs: Ti, Nb, and Ta) and heavy rare earth elements (HREEs) were not transported by the aqueous fluid. These results are consistent with the previous experiments of serpentine dehydration [13]. The low mobilities of HFSEs in our experiments could be an underestimation, because the mode of rutile in the run products is similar to that in the starting material (Table 1), whereas the actual subducted oceanic crust may not contain rutile at lower pressures [25]. An additional notable feature is the higher mobilities of Pb, Nd and Rb relative to U–Th, Sm and Sr, respectively.

We compare the results of the present open-system dehydrationexperiments with those of element partitioning between minerals and aqueous fluids. We calculated percentages of trace elements removed by aqueous fluids in the case where the residual phases were completely equilibrated with aqueous fluids during dehydration, using mineral–fluid partition coefficients determined by Brenan et al. [9,10,26]. Partition coefficients for phengite were assumed to be the same as the values for phlogopite–melt partitioning [27]. Weight fractions of residual minerals were calculated using modal composition (Table 1) and mineral densities assuming:

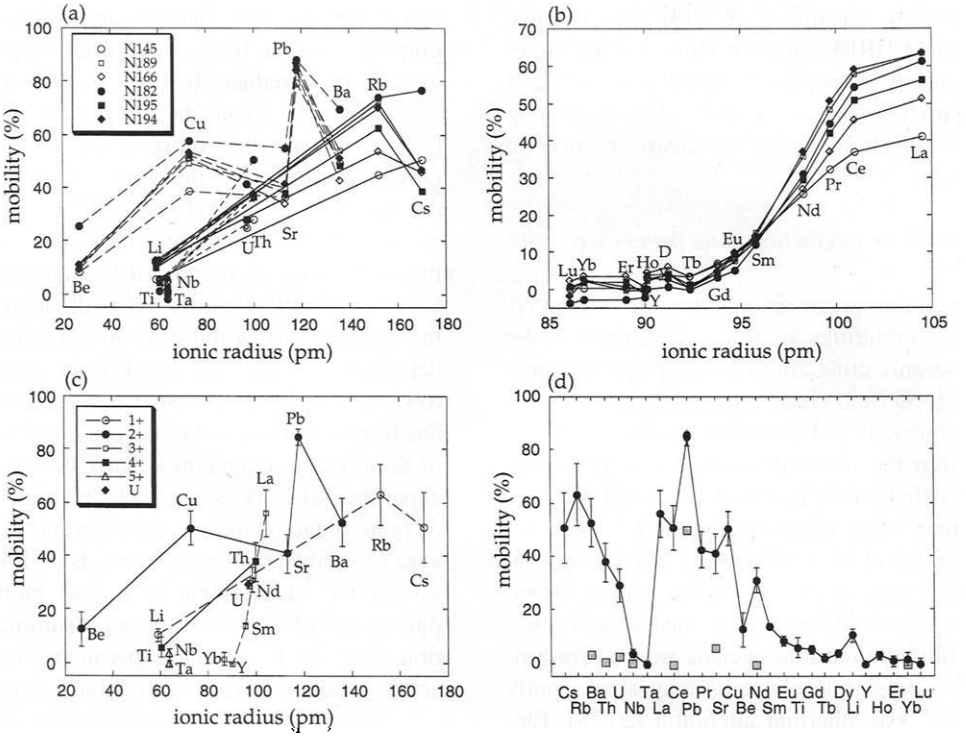

Fig. 2. Mobilities of incompatible trace elements during dehydration experiments potted against ionic radii. Cation coordination was assumed to be 6-fold [42,43]. (a) and (b) Mobilities of incompatible elements during each experiment. (c) Averaged mobilities during six experiments. Error bars indicate standard deviations for six experiments. (d) Comparison of the averaged mobilities in this study (circles) with mobilities assuming mineral–fluid equilibrium partitioning (squares) calculated using mineral–fluid partition coefficients from [9,10,26]. Phengite–fluid partition coefficients are assumed to be the same as phlogopite–melt partition coefficients [27]. Weight fractions of residual minerals are calculated using modal composition (Table 1) and assuming mineral densities as follows: garnet, 3.9 g/cm^3; omphacite, 3.3 g/cm^3; phengite, 2.8 g/cm^3; rutile, 4.3 g/cm^3; and coesite, 2.9 g/cm^3.

3.9 g/cm^3 for garnet, 3.3 g/cm^3 for omphacite, 2.8 g/cm^3 for phengite, 4.3 g/cm^3 for rutile, and 2.9 g/cm^3 for coesite. The calculated "equilibrium" mobilities for incompatible elements are plotted in Fig. 2d. In the case of solid–fluid equilibrium dehydration, LILEs, except for Pb, and HFSEs may be largely retained in the residue, because of their relatively high mineral–fluid partition coefficients (e.g., $D^{cpx-fluid}$ for Sr = ~ 0.5, $D^{garnet-fluid}$ for U = ~ 0.8 [9]) and the low fraction of fluid released (~ 2 wt%). However, Pb could be largely removed by the fluid during equilibrium dehydration because of its low mineral–fluid partition coefficients (< 0.01 for garnet and clinopyroxene [9]). This is consistent with the exceptionally high mobility of Pb relative to other LILEs in the present experiments.

These observations suggest that element transport during open-system dehydration may be related to their abilities to dissolve into aqueous fluids, and not be completely controlled by equilibrium partitioning between fluids and residual solid phases. HFSEs and HREEs, which are highly compatible to the residual phases, were not removed from the residual eclogite in the present open-system experiments, suggesting that these elements were effectively partitioned into the residual phases. However, LILEs and LREEs were more largely transported by the fluid in the present open-system experiments than expected in solid–fluid equilibrium partitioning (Fig. 2d), indicating that LILEs and LREEs were removed by the fluid before equilibrium between the fluid and solid phases was attained. It is thus suggested that LILEs and LREEs may be more readily dissolved into the aqueous fluids than HFSEs and HREEs. Although the low mobilities of HFSEs in our experiments could be affected by the presence of rutile in the

starting material, Tatsumi et al. [13] demonstrated that HFSEs and HREEs are not mobilized by aqueous fluids during serpentinite dehydration, even if rutile and garnet are absent in the residue, suggesting that HFSEs and HREEs may not easily dissolve to aqueous fluids.

3.3. Application to subduction zone processes

The dehydration processes operating in our experiments have similarities to those occurring in the subducted oceanic crust and overlying upper mantle wedge. The H_2O fluid phase released by dehydration reactions is buoyant and therefore migrates upwards separated from the residual solid phases. It is suggested that dehydration reactions in actual subduction zones may occur under open-system conditions. Moreover, actual subducted oceanic crust is not an assemblage of pure minerals but has a dirty signature, because oceanic crust may easily suffer hydrothermal alteration at mid-oceanic ridges. Concentrations of incompatible elements may significantly change during hydrothermal alteration [20,28]. Elements mobilized by such alteration and metamorphic processes may partly remain distributed along the grain boundaries of the residual crystals [11,12,29]. It is likely that incompatible elements in the starting amphibolite are also expected to be partly distributed along the grain boundaries, because the chemical composition and metamorphic grade of the starting material are similar to those of subducted altered MORB. Therefore, it is suggested that the element transport mechanism in the present study may be similar to that operating in subducted oceanic crust, and the element mobilities determined in the present experiments may reflect the whole amounts of elements removed from oceanic crust in subduction zones. This is supported by quantitative calculation in the companion paper [30] demonstrating that the element mobilities can explain the chemical characteristics of typical island arc magmas.

The solubility of U in aqueous fluids is known to be dependent on its oxidation state, with U^{6+} forming more highly soluble complexes than U^{4+}. The oxidation state of U also affects its partition coefficient to silicate minerals [9,31]. Although we did not monitor oxygen fugacity in the experiments, the oxygen fugacity in the charges may have been largely controlled by BN sleeves and plugs within the graphite furnace, because we used perforated Pt foil as sample container. BN may establish the oxygen fugacity lower than the magnetite–wüstite buffer [32]. It follows that most of the U in the charges could be in the U^{4+} state. This may be supported by the low U mobility relative to Th, because U^{6+} is more incompatible to residual phases and may be much more easily mobilized by aqueous fluids than U^{4+} and Th [9]. However, it is difficult to constrain the relevant oxidation state during subduction zone dehydration processes; apart from determining the oxygen fugacity in the asthenospheric mantle, which has been estimated to be one log unit lower than that of the fayalite–magnetite–quartz buffer [33]. Further experimental work is needed to examine the effect of oxygen fugacity during dehydration reactions relevant to subducted oceanic crust. Based on our experiments we suggest that U is less mobile than Pb during dehydration processes, assuming the oxidation state of U in our experiments is relevant to actual subduction zone dehydration processes.

3.4. Origin of HIMU ocean island basalts

Our results indicate that dehydration processes in subduction zones may result in a substantial increase in the U/Pb and Th/Pb ratios of the subducted oceanic crust. This is qualitatively consistent with recycling of dehydrated subducted oceanic crust being able to explain the high U/Pb and Th/Pb ratios of the HIMU source. In detail, it has been proposed that the HIMU source is generated by a mixture of depleted (MORB source) mantle with the ancient subducted oceanic crust, depleted in Pb relative to U and Th by hydrothermal alteration at mid-oceanic ridges and by dehydration processes during subduction [3–5,34]. Furthermore, these authors have estimated that the high Pb isotopic ratios of HIMU require a long ($\sim$ 1–2 Ga) evolution of the HIMU source with U/Pb ratios up to two times those of average N-MORB. The results of this study indicate that U/Pb ratios of the dehydrated basaltic oceanic crust can increase up to more than four times those existing prior to subduction (Fig. 2).

The present experiments also indicate that dehydration processes in subduction zones may result in a decrease in Rb/Sr ratios and a significant increase in

Sm/Nd ratios in the subducted oceanic crust, which leads to low $^{87}Sr/^{86}Sr$ ratios and an increase in $^{143}Nd/^{144}Nd$ ratios of the subducted crust relative to present-day MORB. This is clearly inconsistent with the observed Sr and Nd isotopic composition of HIMU, even given mixing of recycled ancient subducted crust with the depleted MORB source mantle. In existing models for the origin of HIMU [5,6], the Rb/Sr and Sm/Nd ratios of the subducted crust are assumed to remain unfractionated through the subduction process, and it has been concluded accordingly that the Sr and Nd isotopic ratios of the HIMU are consistent with recycling of the subducted oceanic crust. In contrast, Hart and Staudigel [35] have suggested that oceanic crust is strongly enriched in Rb relative to Sr after alteration, and that subduction of highly altered oceanic crust cannot explain the isotopic signature of any OIB, given parent/daughter ratios of the highly altered oceanic crust unfractionated through the subduction process. In order to examine whether the isotopic compositions of the ancient subducted crust can account for isotopic characteristics of the HIMU basalts, we have investigated a simple quantitative model for the isotopic evolution of the ancient subducted basaltic crust based on our experimental data.

3.5. Modeling of the isotopic evolution of the subducted basaltic crust

We shall employ a simple two-stage model for the evolution of the subducted basaltic crust, and assume:

1. the MORB source mantle is a single-stage reservoir with an age of 4.57 Ga derived from the chondritic bulk Earth;
2. the oceanic basaltic crust is derived from the MORB source mantle at various times and is altered at mid-oceanic ridges and on the ocean floor before subduction;
3. the trace-element composition of the oceanic basaltic crust is changed during subduction into the mantle according to the results of our dehydration experiments;

Table 4
Parameters used in the calculation of the evolution of the ancient subducted basaltic crust

	Bulk Earth (primitive mantle)	MORB source	N-MORB	(dehydrated)	Altered MORB	(dehydrated)
Initial ratio (t = 4.57 Ga)						
$^{87}Sr/^{86}Sr$	0.699	0.699				
$^{144}Nd/^{143}Nd$	0.5067	0.5067				
$^{206}Pb/^{204}Pb$	9.307	9.307				
$^{207}Pb/^{204}Pb$	10.294	10.294				
$^{208}Pb/^{204}Pb$	29.476	29.476				
Present ratio						
$^{87}Sr/^{86}Sr$	0.7047	0.7022				
$^{144}Nd/^{143}Nd$	0.51264	0.5133				
$^{206}Pb/^{204}Pb$	17.8	17.3				
$^{207}Pb/^{204}Pb$	15.6	15.4				
$^{208}Pb/^{204}Pb$	38.2	37.1				
$^{87}Rb/^{86}Sr$	0.085	0.048	0.018	0.011	0.316	0.195
$^{147}Sm/^{143}Nd$	0.1966	0.219	0.215	0.264	0.215	0.264
$^{238}U/^{204}Pb$	8.2	7.8	11.2	52.3	22	102.7
$^{232}Th/^{204}Pb$	34	30	29.9	123.6	7.26	30.0
Sr	20	14.7	90	54	180	108
Nd	1.08	0.815	6.68	4.68	6.68	4.68
Pb	0.155	0.016	0.5	0.08	0.8	0.12
Nd/Sr	0.054	0.055	0.074	0.087	0.037	0.043

Isotopic compositions of initial bulk Earth from [49]; those of present bulk Earth from [50–52]. Trace element compositions are: primitive mantle and MORB source from [53]; N-MORB and altered MORB from [28,36–38].

4. the subducted basaltic crust is stored within the mantle, and its evolution from the time of its generation to the present day is approximated by a single-stage evolution curve.

Although the chemical composition of altered oceanic crust is strongly heterogeneous [28], bulk parent/daughter ratios of the altered oceanic crust before dehydration are assumed to be the same as: (1) averaged values of the fresh N-MORB [36,37], and (2) those of altered MORB [28,38]. The former is representative of less-altered oceanic crust, and the latter of highly altered oceanic crust. Composition of the dehydrated oceanic crust was calculated using the averaged mobilities of elements during amphibolite dehydration (Table 3). The parameters used in these calculation are listed in Table 4.

The calculated isotopic compositions of the ancient subducted oceanic crust are shown in Fig. 3. The highly altered oceanic crust could have extremely radiogenic Sr, Nd and Pb isotopes, far from those of the HIMU component. This suggests that the highly altered oceanic crust is not suitable for the source material of the HIMU component, because the isotopic composition of the HIMU component cannot be produced even if the highly altered oceanic crust of any age is mixed with the depleted mantle or more enriched mantle to any extent. In contrast, the less altered oceanic crust has less radiogenic Sr isotopes and more radiogenic Nd and Pb isotopes than the present MORB and all OIB suites. The subducted, less altered, oceanic crust may develop extremely high Pb isotopic ratios, sufficient to account for those of HIMU: the Pb isotopic ratios of the HIMU component could be produced by mixing of the ancient less altered oceanic crust of ~ 1–2 Ga old with the present depleted (MORB-source-like) mantle or the primitive (bulk-Earth-like) mantle (Fig. 3, upper two). However, Sr–Nd mixing curves of recycled oceanic crust with any mantle component convex upward (Fig. 3, lowest), reflecting higher Nd/Sr ratios of dehydrated oceanic crust relative to the primitive mantle (Table 4). It follows that Sr and Nd isotopic ratios of HIMU cannot be produced by bulk addition of the less altered oceanic crust to the present depleted or primitive mantle.

The results described above, however, do not preclude involvement of the subducted oceanic crust in the HIMU source. A mixture of subducted oceanic

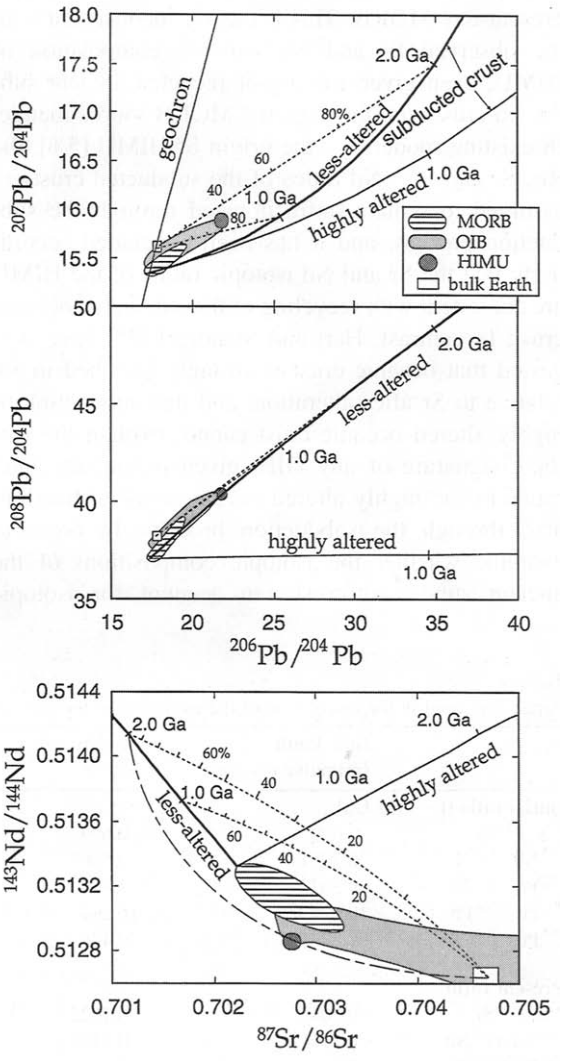

Fig. 3. Isotope diagrams showing calculated compositions of the ancient subducted oceanic crust for, from top to bottom: $^{206}Pb/^{204}Pb$–$^{207}Pb/^{204}Pb$; $^{206}Pb/^{204}Pb$–$^{208}Pb/^{204}Pb$; and $^{87}Sr/^{86}Sr$–$^{143}Nd/^{144}Nd$. Bold lines indicate present isotopic-compositions of the subducted less-altered oceanic crust; thin lines indicate those of the subducted highly altered crust. Numbers on the solid lines are ages of the formation of the oceanic crust. Dotted lines are mixing curves of the subducted 1 Ga and 2 Ga old basaltic crust with the present primitive mantle. Numbers on the dotted lines are percentages of the subducted crust in the mixture. The short-long dashed line in the figure at the bottom shows a mixing curve assuming $(Nd/Sr)_{subducted\ crust}/(Nd/Sr)_{mantle} = 0.10$, which could explain the Sr and Nd isotopic compositions of HIMU.

crust with primitive (bulk-Earth like) mantle could produce isotopic compositions similar to that of HIMU if the ratio $(Nd/Sr)_{subducted\ crust}/(Nd/Sr)_{mantle}$ is reduced to about 0.10 (Fig. 3, lowest). This requires a component with Sr and Nd isotopic ratios similar to ancient subducted oceanic crust, but with Nd/Sr ratios 90% lower than in subducted oceanic crust. Such a component is possible to be generated by processes including contribution of subducted oceanic crust. A recent study of seismic anisotropy in the D″ layer [39] suggests a possibility of partial melting of subducted oceanic crust in the lowermost mantle. This implies that the HIMU source does not necessarily have trace element ratios similar to those of subducted oceanic crust, even if the HIMU source involves subducted oceanic crust. Trace element characteristics of HIMU basalts, such as higher Nb/Zr ratios than other OIBs, cannot be explained by simple mixing of subducted oceanic crust with the primitive mantle nor partial melting in the upper mantle [40], suggesting that element fractionation in the presence of perovskite under lower mantle conditions are required to generate the HIMU reservoir, by involvement of subducted oceanic crust. On the other hand, major element characteristics of HIMU basalts indicate that the HIMU source is more enriched in a basaltic component than in those of non-HIMU basalts, implying the contribution of the subducted oceanic crust in the formation of the HIMU source [40]. Isotope signatures of OIB suites suggest that mantle sources of OIBs are likely to contain relatively primitive components from the lower mantle [41]. This implies that the HIMU source involves significant amounts of primitive components. Although element partitioning between minerals and silicate melt under lower mantle conditions are not sufficiently determined, possible processes to produce the HIMU source may include partial melting of subducted crust in the lower mantle and refertilization of primitive mantle material by the melts from the subducted crust, as suggested by Kogiso et al. [40].

4. Conclusions

The amphibolite dehydration experiments documented that elements with larger ionic radii are more readily transported by aqueous fluids during open-system dehydration processes. The results indicate that dehydration of subducted oceanic crust may result in large increases in U/Pb and Th/Pb, although there is still uncertainty about the oxidation state of U during subduction zone dehydration processes. Dehydration reactions in subduction zones also result in large increases in the Sm/Nd ratio and a decrease in the Rb/Sr ratio of subducted oceanic crust.

The U/Pb and Th/Pb ratios of the dehydrated oceanic crust may be able to explain the high Pb isotopic ratios of HIMU, given sufficiently long periods of isolation in the mantle. In contrast, dehydrated oceanic crust may have higher Nd isotopic ratios and lower Sr isotopic ratios than the present MORB source mantle, indicating that Sr and Nd isotopic ratios of HIMU cannot be readily explained by simple bulk mixing of the ancient subducted oceanic crust with depleted or primitive mantle. This requires significant fractionation of Nd/Sr ratios in the subducted oceanic crust in the deep mantle before mixing with mantle material to produce the HIMU reservoir.

Acknowledgements

We are very grateful to T. Taniguchi, S. Yamaoka and H. Yamada in the National Institute for Research in Inorganic Materials for their great help in high-pressure experiments. We wish to acknowledge S. Eggins for analyzing our samples at ANU, and many helpful discussions. We also thank J. Brenan, M. Johnson, and E. Hauri for their constructive reviews. This work was supported by Research Fellowships of the Japan Society for the Promotion of Science for Young Scientists to TK, and Grants-in-Aid from the Ministry of Education, Science and Culture of Japan (05231106 and 08404029) and a Special Coordination Fund for Promoting Science and Technology (Superplume) from the Science and Technology Agency of Japan to YT. *[CL]*

References

[1] Y. Tatsumi and S.M. Eggins, Subduction Zone Magmatism, 211 pp., Blackwell, Cambridge, 1995.

[2] A.W. Hofmann and W.M. White, Mantle plumes from ancient oceanic crust, Earth Planet. Sci. Lett. 57, 421–436, 1982.
[3] C. Dupuy, P. Vidal, H.G. Barsczus and C. Chauvel, Origin of basalts from the Marquesas Archipelago (south central Pacific Ocean): isotope and trace element constraints, Earth Planet. Sci. Lett. 82, 145–152, 1987.
[4] B.L. Weaver, The origin of ocean island basalt end-member compositions: trace element and isotopic constraints, Earth Planet. Sci. Lett. 104, 381–397, 1991.
[5] C. Chauvel, A.W. Hofmann and P. Vidal, HIMU-EM: The French Polynesian connection, Earth Planet. Sci. Lett. 110, 99–119, 1992.
[6] E.H. Hauri and S.R. Hart, Re–Os isotope systematics of HIMU and EMII oceanic island basalts from the south Pacific Ocean, Earth Planet. Sci. Lett. 114, 353–371, 1993.
[7] M. Roy-Barman and C.J. Allègre, $^{187}Os/^{185}Os$ in oceanic island basalts: tracing oceanic crust recycling in the mantle, Earth Planet. Sci. Lett. 129, 145–161, 1995.
[8] A. Zindler and S. Hart, Chemical geodynamics, Ann. Rev. Earth Planet. Sci. 14, 493–571, 1986.
[9] J.M. Brenan, H.F. Shaw, F.J. Ryerson and D.L. Phinney, Mineral–aqueous fluid partitioning of trace elements at 900°C and 2.0 GPa: constraints on the trace element chemistry of mantle and deep crustal fluids, Geochim. Cosmochim. Acta 59, 3331–3350, 1995.
[10] J.M. Brenan, H.F. Shaw and F.J. Ryerson, Experimental evidence for the origin of lead enrichment in convergent-margin magmas, Nature 378, 54–56, 1995.
[11] F.A. Frey and D.H. Green, The mineralogy, geochemistry and origin of lherzolite inclusions in Victoria basanites, Geochim. Cosmochim. Acta 38, 1023–1059, 1974.
[12] A.R. Basu and V.R. Murthy, Ancient lithospheric lherzolite xenolith in alkali basalt from Baja California, Earth Planet. Sci. Lett. 35, 239–246, 1977.
[13] Y. Tatsumi, D.L. Hamilton and R.W. Nesbitt, Chemical characteristics of fluid phase released from a subducted lithosphere and origin of arc magmas: evidence from high-pressure experiments and natural rocks, J. Volcanol. Geotherm. Res. 29, 293–309, 1986.
[14] C.P. Hess, Thermodynamics of thin fluid films, J. Geophys. Res. 90, 7219–7229, 1994.
[15] A. Miyashiro, Metamorphism and Metamorphic Belts, 492 pp., Allen and Unwin, London, 1973.
[16] Y. Tatsumi, Migration of fluid phases and genesis of basalt magmas in subduction zones, J. Geophys. Res. 94, 4697–4707, 1989.
[17] S.M. Peacock, The importance of blueschist → eclogitedehydration reactions in subducting oceanic crust, GSA Bull. 105, 684–694, 1993.
[18] S. Poli, The amphibolite–eclogite transformation: anexperimental study on basalt, Am. J. Sci. 293, 1061–1107, 1993.
[19] S. Poli and M.W. Schmidt, Water transport and release in subduction zones: experimental constraints on basaltic and andesitic systems, J. Geophys. Res. 100, 22,299–22,314, 1995.
[20] J.C. Alt, J. Honnorez, C. Laverne and R. Emmermann, Hydrothermal alteration of a 1 km section through the upper oceanic crust, deep see drilling project hole 504B: mineralogy, chemistry, and evolution of seawater–basalt interactions, J. Geophys. Res. 91, 10309–10335, 1986.
[21] S.M. Eggins, J.D. Woodhead, L. Kinsley, M.T. McCulloch and J. Hergt, A precise method for ICP–MS analysis of geological samples employing enriched isotope internal standards: applications to subduction zone magmas, Chem. Geol., in press.
[22] J.P. Lorand, Are spinel lherzolite xenoliths representative of the abundance of sulfur in the upper mantle?, Geochim. Cosmochim. Acta 54, 1487–1492, 1990.
[23] T. Irifune and A.E. Ringwood, Phase transformations in a harzburgite composition to 26 GPa: Implications for dynamical behaviour of the subducting slab, Earth Planet. Sci. Lett. 86, 365–376, 1987.
[24] M.W. Schmidt, Experimental constraints on recycling of potassium from subducted oceanic crust, Science 272, 1927–1930, 1996.
[25] T.H. Green, Experimental evidence for the role of accessory phases in magma genesis, J. Volcanol. Geotherm. Res. 10, 405–422, 1981.
[26] J.M. Brenan, H.F. Shaw, D.L. Phinney and R.J. Ryerson, Rutile–aqueous fluid partitioning of Nb, Ta, Hf, Zr, U and Th: implications for high field strength element depletion in island-arc basalts, Earth Planet. Sci. Lett. 128, 327–339, 1994.
[27] T. LaTourrette, R.L. Hervig and J.R. Holloway, Trace element partitioning between amphibole, phlogopite, and basanite melt, Earth Planet. Sci. Lett. 135, 13–30, 1995.
[28] H. Staudigel, G.R. Davies, S.R. Hart, K.M. Marchant and B.M. Smith, Large scale isotopic Sr, Nd and O isotopic anatomy of altered oceanic crust: DSDP/ODP sites 417/418, Earth Planet. Sci. Lett. 130, 169–185, 1995.
[29] A. Zindler and E. Jagoutz, Mantle cryptology, Geochim. Cosmochim. Acta 52, 319–333, 1988.
[30] Y. Tatsumi and T. Kogiso, Trace element transport during dehydration processes in the subducted oceanic crust: 2. Origin of chemical characteristics in arc magmas, Earth Planet. Sci. Lett. 148 (this issue), 1997.
[31] P. Beattie, The generation of uranium series disequilibria by partial melting of spinel peridotite: constraints from partitioning studies, Earth Planet. Sci. Lett. 117, 379–391, 1993.
[32] R.F. Wendlandt, J.S. Huebner and W.J. Harrison, The redox potential of boron nitride and implications for its use as a crucible material in experimental petrology, Am. Mineral. 67, 170–174, 1982.
[33] C. Ballhaus, Redox state of lithospheric and asthenospheric upper mantle, Contrib. Mineral. Petrol. 114, 331–348, 1993.
[34] C.G. Chase, Oceanic island Pb: two-stage histories and mantle evolution, Earth Planet. Sci. Lett. 52, 227–284, 1981.
[35] S.R. Hart and H. Staudigel, Isotopic characterization and identification of recycled components, in: Crust/Mantle Recycling at Convergence Zones, S.R. Hart and L. Gülen, eds., NATO ASI Ser. C 258, pp. 15–28, Kluwer, Dordrecht, 1989.

[36] A.W. Hofmann, Chemical differentiation of the Earth: the relationship between mantle, continental crust, and oceanic crust, Earth Planet. Sci. Lett. 90, 297–314, 1988.
[37] W.M. White, $^{238}U/^{204}Pb$ in MORB and open system evolution of the depleted mantle, Earth Planet. Sci. Lett. 115, 211–226, 1993.
[38] M.T. McCulloch and J.A. Gamble, Geochemical and geodynamical constraints on subduction zone magmatism, Earth Planet. Sci. Lett. 102, 358–374, 1991.
[39] J.-M. Kendall and P.G. Silver, Constraints from seismic anisotropy on the nature of the lowermost mantle, Nature 381, 409–412, 1996.
[40] T. Kogiso, Y. Tatsumi, G. Shimoda and H.G. Barsczus, HIMU ocean island basalts in southern Polynesia: new evidence for whole-mantle scale recycling of subducted oceanic crust, J. Geophys. Res., in press.
[41] S.R. Hart, E.H. Hauri, L.A. Oschmann and J.A. Whitehead, Mantle plumes and entrainment: isotope evidence, Science 256, 517–520, 1992.
[42] R.D. Shannon and C.T. Prewitt, Effective ionic radii in oxides and fluorides, Acta Crystallogr. B25, 925–946, 1969.
[43] R.D. Shannon and C.T. Prewitt, Revised values of effective ionic radii, Acta Crystallogr. B26, 1046–1048, 1970.
[44] J.C. Alt and R. Emmermann, Geochemistry of hydrothermally altered basalts: Deep Sea Drilling Project hole 504B, Leg 83, Init. Rep. DSDP, pp. 249–262, Washington, DC, 1983.
[45] F.A. Frey, W.B. Bryan and G. Thompson, Atlantic Ocean floor: geochemistry and petrology of basalts from legs 2 and 3 of the Deep-Sea Drilling Project, J. Geophys. Res. 79, 5507–5527, 1974.
[46] S.E. Humphris and G. Thompson, Hydrothermal alteration of oceanic basalts by seawater, Geochim. Cosmochim. Acta 42, 107–125, 1978.
[47] S.E. Humphris and G. Thompson, Trace element mobility during hydrothermal alteration of oceanic basalts, Geochim. Cosmochim. Acta 42, 127–136, 1978.
[48] H. Staudigel, S.R. Hart and S.H. Richardson, Alteration of the oceanic crust: processes and timing, Earth Planet. Sci. Lett. 52, 311–327, 1981.
[49] M.T. McCulloch and L.P. Black, Sm–Nd isotopic systematics of Enderby Land granulites and evidence for the redistribution of Sm and Nd during metamorphism, Earth Planet. Sci. Lett. 71, 46–58, 1984.
[50] S.L. Goldstein, R.K. O'Nions and P.J. Hamilton, A Sm–Nd study of atmospheric dusts and particulates from major river systems, Earth Planet. Sci. Lett. 70, 221–236, 1984.
[51] S.R. Taylor and S.M. McLennan, The Continental Crust: its Composition and Evolution, Blackwell, Oxford, 1985.
[52] C.J. Allègre, E. Lewin and B. Dupré, A coherent crust–mantle model for the uranium–thorium–lead isotopic system, Chem. Geol. 70, 211–234, 1988.
[53] D. McKenzie and R.K. O'Nions, The source regions of ocean island basalts, J. Petrol. 36, 133–159, 1995.